Global String Radiation

R. A. Battye and E. P. S. Shellard

Department of Applied Mathematics and Theoretical Physics University of Cambridge Silver Street, Cambridge epss @ amtp.cam.ac.uk Paper submitted to Nuclear Physics B.

Abstract

We study Goldstone boson (or axion) radiation from global U(1)-strings making direct quantitative comparisons between numerical scalar field theory simulations and linearized analytic calculations in the dual antisymmetric tensor representation. Concentrating on periodic long string configurations, we show excellent correspondence for both the amplitude and spectrum of radiation. We also find good agreement with a linearized analytic model for radiation backreaction, demonstrating that damping due to the lowest n=2 harmonic is effective in strongly suppressing higher harmonics. This work establishes the validity of the Kalb-Ramond action in describing low-energy global string dynamics, along with the associated self-field renormalization of the equations of motion. We also describe the different nature of massive radiation from high curvature regions and the collapse and annihilation of a circular loop. As an application in axion models, we discuss the relative loop and long string radiation contribution to a cosmological bound on the axion mass. A parallel linearized formalism for gravitational radiation is also provided.

1 Introduction

Global strings are associated with the breaking of a global symmetry that leaves a degenerate vacuum manifold which is not simply-connected. Global strings arise naturally in a variety of physical contexts; they are generic in axion models and seemingly also in superstring theories, and they can appear in GUT models, for example, through the breaking of a global B-L symmetry. For appropriate mass scales, global strings can take on many of the cosmological roles invoked for local gauge strings. Despite these similarities, the literature on global strings is sparse and their physics is inadequately understood and often even misunderstood. The chief distinction is that, unlike local strings which radiate gravitationally, oscillating global strings decay more rapidly into massless Goldstone bosons. It is the nature and characterization of this radiation which forms the subject of this paper.

The popularity of the axion in particle physics and cosmology has provided one of the main motivations for studying global strings, so it is enlightening to provide a context for this discussion. The imposition of an extra global $U(1)_{PQ}$ symmetry remains the most elegant solution to the strong CP-problem of QCD [PQ]. This

Peccei-Quinn symmetry is broken at some high energy scale f_a and the corresponding pseudo-Goldstone boson ϑ which appears is the axion [Wil, Wei]. The axion field ϑ in these extended models becomes directly related to the previously arbitrary $\bar{\theta}$ -parameter of QCD which is associated with any CP-violation. At the QCD-scale, "soft" instanton effects slightly tilt the symmetry breaking potential and the axion acquires a small mass m_a . The minimum of the potential then becomes $\vartheta = 0$ which corresponds to the CP-conserving value for $\bar{\theta}$. Note that neutron electric dipole measurements imply that $\bar{\theta} < 10^{-10}$.

In general, the couplings of the axion to ordinary matter are inversely proportional to the symmetry breaking scale $f_{\rm a}$. By making $f_{\rm a}$ sufficiently large, the axion becomes effectively "invisible." A lower bound for $f_{\rm a}$ is provided in astrophysical contexts by axion production because, being so weakly interacting, they can escape from the entire volume of a star and compete with surface photon or neutrino losses. A study of red giant cooling provides the limit $f_{\rm a} > 10^9 \, {\rm GeV} \, [RG]$, while supernova 1987a implies $f_{\rm a} \gtrsim 10^{10} \, {\rm GeV} \, [SN]$.

As one of the prime cold dark matter candidates, the cosmology of the axion has attracted considerable interest. Requiring that the density contribution of axions is below critical (that is, $\Omega_{\rm a} < 1$) provides an upper bound on $f_{\rm a}$. If the universe passes normally through the Peccei-Quinn phase transition, then there are a number of possible sources of axions. Thermal axions produced by the phase transition are massless and are redshifted away by the expansion. Another source is the production of axions through oscillations about the minimum of the potential $\vartheta = 0$ due to initial homogeneous misalignments of the axion above $T > \Lambda_{\rm QCD}$. These zero-momentum axions were estimated to give the relative energy density, [AS, PWW],

$$\Omega_a \approx 0.9 \times 10^{\pm 0.5} \left(\frac{f_a}{10^{12} GeV}\right) \bar{\theta}_i^2 \tag{1}$$

where $\bar{\theta}_i$ is the initial average misalignment angle.* These axions were mistakenly thought to be the only significant contribution to the axion density, imposing the upper bound

$$f_a \lesssim 10^{12} GeV. (2)$$

This cosmological estimate ignored topological effects at the Peccei-Quinn phase transition [VE], that is, the inevitable production of global $U_{PQ}(1)$ -strings through the Kibble mechanism.† Davis [Dava, Davb] suggested that the radiative decay of the global string network provided a more significant contribution to the

^{*} Note that this bound can be weakened if there is substantial entropy production at some time between the QCD scale and nucleosynthesis, for example, by engineering the out-of-equilibrium decay of a massive particle species (such as ref. [Lyth1]).

[†] We should point out here that it is possible to avoid axion strings altogether through inflation, though such models may have unsatisfactory aspects. If f_a is pushed above a GUT scale reheat temperature, we must by (2) anthropically arrange a small misalignment angle $\bar{\theta}_i$ in our region of the universe. The alternative of a low reheat temperature below 10^{12} GeV assumes baryogenesis at the electroweak

axion density. This was estimated by assuming that direct radiation by long strings into the fundamental harmonic was the primary energy loss mechanism. Long string radiation was subsequently studied in more detail by Davis & Shellard [DSa] who demonstrated that strings radiate with a classical spectrum, predominantly in the second harmonic. Applying this spectrum with the previous assumptions and numerical results from network evolution, they deduced a cosmological bound

$$f_a \lesssim 10^{10} GeV \,, \tag{3}$$

which is two orders of magnitude stronger than the zero-momentum bound from (1). A comparison with the astrophysical constraint brought into question the viability of axion models in such scenarios, suggesting that inflation may be required to eliminate axion strings.

There are, however, further contributions to the axion density. When the axion mass switches on at $T = \Lambda_{\rm QCD}$, the S^1 vacuum manifold is tilted, and the minima lie at the discrete values $\vartheta = 0, \pm 2\pi, \pm 4\pi, ...$ Thick domain walls form in regions where there are large variations in the axion field ϑ [Sika]. In particular, strings become attached to domain walls which begin to dominate the dynamics of the string network [VE]. Reconnections between strings and domain walls facilitate the rapid decay and annihilation of the hybrid system into more axions, as demonstrated numerically [Sa,PRS,Sb]. These additional axions will serve to strengthen the bound (3). Paradoxically, axions produced by loops will tend to weaken the bound (3), which was derived assuming only long string radiation. If axions come predominantly from small loops instead of long strings, they will be produced at higher frequencies and so lose more of their relativistic energy through redshifting [Sb]. We shall return briefly to this issue in Appendix A, leaving detailed analysis for a future publication.

The orthodox classical understanding of string radiation assumed above has been challenged by Sikivie and coworkers who have raised a number of important issues [HarS, HagS, Sikb]. As we shall point out in §2, the global string appears to be a non-local object with logarithmic contributions to its energy density coming from the Goldstone boson field on all length scales above the string core width δ . Implicit in radiation calculations, therefore, is the assumption that the global string maintains its integrity during its motion, and that these less localized components merely renormalize the string tension (provided that they are on length scales below the string curvature radius). Harari & Sikivie [HarS] questioned this renormalization and suggested that the string core during its motion somehow decouples from the surrounding "cloud" of Goldstone bosons. They proposed that the global string was in fact critically damped and lost all its oscillation energy in less than one period, implying that the radiation power spectrum was flat with contributions at all wavelengths above δ . These suggestions were supported by later numerical

scale and may be ruled out in future by constraining the possible shape of the inflaton potential using microwave anisotropies, given that one knows the relative contribution of gravity waves [CKLL].

simulations of perfectly circular loops which, by virtue of their symmetry, are in fact expected to behave in this manner [HagS]. If verified, a flat radiation spectrum would lead to a cosmological constraint, $f_a \lesssim 10^{12} \text{GeV}$ which is comparable to the zero-momentum bound (2) but at variance with original string bound (3).

Here, we endeavour to settle this controversy beyond reasonable doubt; we make an extensive study employing sophisticated numerical techniques which we compare quantitatively with the analytic formalism developed to describe global strings. This formalism using two-index antisymmetric tensors [Wit, VVa, DSb] has been used to study radiation from loop trajectories [VVa, DQ] and periodic long strings [Saka]. We point out where our analysis differs from previous work and we introduce a simple backreaction model, based on the analytic methods, as a first step in describing the damping of small-scale structure on cosmic strings. Resolution of these questions is all the more pertinent because of ongoing and proposed axion dark matter searches. The motivation for these expensive experiments relies heavily on the theoretically predicted parameter range allowed by the cosmological bounds (2) and (3).

Throughout this paper we employ a (+--) signature for the spacetime metric $g_{\mu\nu}$, (+-) for the induced metric on the string worldsheet γ_{ab} , the coordinates for which are given by $X^{\mu} = X^{\mu}(\sigma, \tau)$, with the null coordinates, $u = \sigma - \tau$, $v = \sigma + \tau$.

2 Analytic formalism

The Goldstone model

The essential features of global strings are exhibited in the simple U(1) Goldstone model with action given by,

$$S = \int d^4x \left\{ \partial_{\mu} \bar{\Phi} \partial^{\mu} \Phi - \frac{1}{4} \lambda (\bar{\Phi} \Phi - f_{\rm a}^2)^2 \right\}$$

$$= \int d^4x \left\{ (\partial_{\mu} \phi)^2 + \phi^2 (\partial_{\mu} \vartheta)^2 - \frac{1}{4} \lambda (\bar{\Phi} \Phi - f_{\rm a}^2)^2 \right\}, \tag{4}$$

where Φ is a complex scalar field which has been split as $\Phi = \phi e^{i\vartheta}$ into a massive (real) Higgs component ϕ and a massless (real periodic) Goldstone boson ϑ . The corresponding Euler-Lagrange equations are given by

$$\partial_{\mu}\partial^{\mu}\Phi + \frac{1}{2}\lambda\Phi(\bar{\Phi}\Phi - f_{\rm a}^2) = 0.$$
 (5)

For a straight global string lying along the z-axis, we take the ansatz

$$\Phi(r,\theta) = \phi(r)e^{in\theta}, \qquad (6)$$

where θ is the azimuthal angle and n is the winding number. We take the usual boundary conditions, $\phi(0) = 0$ and $\phi \to f_a$ as $r \to \infty$. Despite these conditions, the energy per unit length μ is mildly divergent (n=1),

$$\mu(\Delta) \approx \mu_0 + \int_{\delta}^{\Delta} \left[\frac{1}{r} \frac{\partial \Phi}{\partial \theta} \right]^2 2\pi r \, dr \approx \mu_0 + 2\pi f_{\rm a}^2 \ln \left(\frac{\Delta}{\delta} \right) ,$$
 (7)

where $\delta \sim (\sqrt{\lambda} f_{\rm a})^{-1}$ is the string core width and $\mu_0 \sim f_{\rm a}^2$ is the core energy associated with the massive field ϕ (that is, within $r \lesssim \delta$). The length-scale Δ is the renormalisation scale provided in general by the curvature radius of the string or the average inter-string separation. Typically, at the present day with $f_{\rm a} \sim 10^{12} {\rm GeV}$ the logarithm in (7) is $\ln(\Delta/\delta) \approx 70$. This implies that there is much more energy in the Goldstone field than in the string core μ_0 , a fact which has made the understanding of global strings intuitively hazardous.

Dual representation: antisymmetric tensors

The analytic treatment of global string dynamics is hampered by the topological coupling of the string to the Goldstone boson. However, we can exploit the well-known duality between a massless scalar field and a two-index antisymmetric tensor field $B_{\mu\nu}$ to replace the Goldstone boson ϑ in (4) via the relation,

$$\phi^2 \partial_\mu \vartheta = \frac{1}{2} f_a \epsilon_{\mu\nu\lambda\rho} \partial^\nu B^{\lambda\rho} \,. \tag{8}$$

The transformation in the presence of vortices where $\phi \to 0$ has to be performed carefully [DSb], (4) then becomes

$$S = \int d^4x \left\{ (\partial_{\mu}\phi)^2 - \frac{f_a^2}{6\phi^2} H^2 - \frac{1}{4}\lambda(\phi^2 - f_a^2)^2 \right\} - 2\pi f_a \int B_{\mu\nu} d\sigma^{\mu\nu} , \qquad (9)$$

where the field strength tensor is $H^{\mu\nu\lambda} = \partial^{\mu}B^{\nu\lambda} + \partial^{\lambda}B^{\mu\nu} + \partial^{\nu}B^{\lambda\mu}$ and the area element $d\sigma^{\mu\nu}$ is given in terms of the worldsheet $X(\sigma,\tau)$ swept out by the zeroes of the Higgs field $(\phi = 0)$,

$$d\sigma^{\mu\nu} = \epsilon^{ab} \partial_a X^{\mu} \partial_b X^{\nu} d\sigma d\tau \,. \tag{10}$$

Effectively, the string acts as a source term for $B^{\mu\nu}$ with a current density given by

$$J^{\mu\nu} = \frac{f_{\rm a}}{2} \int \delta^{(4)}[x - X(\sigma, \tau)] \, d\sigma^{\mu\nu} \,. \tag{11}$$

Integrating radially over the massive degrees of freedom in (9) yields the Kalb-Ramond action [KR],

$$S = -\mu_0 \int \sqrt{-\gamma} \, d\sigma d\tau - \frac{1}{6} \int d^4x \, H^2 - 2\pi f_a \int B_{\mu\nu} d\sigma^{\mu\nu} \,. \tag{12}$$

The first term is the familiar Nambu action for local strings, the second term is the antisymmetric tensor field strength for both external fields and the self-field of the string, and the last term is a contact interaction between the $B^{\mu\nu}$ field and the string worldsheet. The coupling between the string and $B_{\mu\nu}$ is analogous to the electromagnetic coupling of a charged particle, and is amenable to the same calculational techniques.

Varying the action (12) with respect to X^{μ} and $B_{\mu\nu}$ gives the equations of motion for the string and the antisymmetric tensor field,

$$\mu_0(\ddot{X}^{\mu} - X''^{\mu}) = 2\pi f_a H^{\mu\alpha\beta} (\dot{X}_{\alpha} X'_{\beta} - X'_{\alpha} \dot{X}_{\beta}), \qquad (13)$$

$$\partial^{\alpha}\partial_{\alpha}B_{\mu\nu} = 2\pi f_a \int d\sigma d\tau (\dot{X}_{\mu}X'_{\nu} - X'_{\mu}\dot{X}_{\nu})\delta^{(4)}(x - X(\sigma, \tau)), \qquad (14)$$

where we have employed the conformal string gauge and the Lorentz antisymmetric tensor gauge,

$$\dot{X}^2 + X'^2 = 0,$$

 $\dot{X}.X' = 0,$
 $\partial_{\mu}B^{\mu\nu} = 0.$ (15)

As for the electron we have to perform a renormalization because the antisymmetric tensor field comprises both the self-field and the radiation field of the string. The self-field is logarithmically divergent but it can be absorbed such that [LR, DQ]

$$\mu(\Delta)(\ddot{X}^{\mu} - X^{\prime\prime\mu}) = f^{\mu} \tag{16}$$

where Δ is the renormalisation scale introduced in (7) and f^{μ} is the finite radiation backreaction force on the string. The exact form and effect of the radiation backreaction force term is the subject of another publication [BSb].

The renormalised equations of motion (16) for the string, assuming the effects of radiation backreaction to be small, that is $f^{\mu} \simeq 0$ can be approximated by the Nambu equations of motion. Using the conformal gauge (15), these equations of motion have the general solution

$$X^{0} = t = \tau, \quad \mathbf{X} = \frac{1}{2} \left[\mathbf{a}(u) + \mathbf{b}(v) \right], \tag{17}$$

where u and v are null coordinates on the worldsheet and

$$\mathbf{a}^{\prime 2} = 1, \quad \mathbf{b}^{\prime 2} = 1.$$
 (18)

These equations have closed loop solutions and long (or infinite) string solutions. Fig. 1 illustrates two different long string solutions which are periodic and will be employed in our subsequent analysis.

Radiation calculations using antisymmetric tensors

Methods developed for calculating gravitational radiation from strings [Tur, VVb] [Bur] are readily applied to an antisymmetric tensor field radiation [VVa]. This work focussed on loop radiation, but the formalism has also been adapted for the study of long strings, that is, infinitely long periodic sources [Saka, Sakb]. Given a periodicity length L in both σ and τ , then along a z-directed string we can write $X^3 = \alpha \sigma + P_1(u) + P_2(v)$, where the functions P_1 and P_2 are also periodic with period L and assumed to be small relative to α . By analogy with the gravitational

Figure 1: Some specific periodic long string solutions: (a) helix, (b) pure sine wave

radiation analysis [Saka], one can deduce that the average power radiated per unit length by the string is

$$\frac{dP}{dz} = 2\pi \sum_{n=1}^{\infty} \omega_n \sum_{|\kappa_m| < \alpha \omega_n} \int_0^{2\pi} d\varphi \, \widetilde{J}^{\mu\nu*}(\omega_n, \mathbf{k}^{\perp}, \kappa_m) \, \widetilde{J}_{\mu\nu}(\omega_n, \mathbf{k}^{\perp}, \kappa_m) \,, \qquad (19)$$

where $\omega_n = 2\pi n/L$, $\kappa_m = 2\pi m/\alpha L$, $\mathbf{k}^{\perp} = |\mathbf{k}^{\perp}|(\cos\varphi, \sin\varphi)$, $|\mathbf{k}^{\perp}| = \sqrt{\omega_n^2 - \kappa_m^2}$ and $\widetilde{J}^{\mu\nu}$ is the Fourier transform of the source distribution $J^{\mu\nu}$ given by (11). Using the split into left- and right-movers for $J^{\mu\nu}$ derived in Apppendix B one can deduce that

$$\frac{dP}{dz} = \frac{8\pi^2 f_a^2}{\alpha^2 L} \sum_{n=1}^{\infty} n \sum_{\substack{|m| < \alpha n \\ m \text{ or } n \text{ or } n}} \int_0^{2\pi} d\varphi \{|U|^2 |V|^2 - |U^* \cdot V|^2\},$$
 (20)

where

$$U^{\mu} = \int_{0}^{L} \frac{du}{L} \partial_{u} X_{R}^{\mu} e^{-ik.X_{R}(u)},$$

$$V^{\mu} = \int_{0}^{L} \frac{dv}{L} \partial_{v} X_{L}^{\mu} e^{-ik.X_{L}(v)}$$

$$k^{\mu} = (\omega_{n}, \mathbf{k}^{\perp}, \kappa_{m}).$$
(21)

As described in the previous section, the antisymmetric tensor notation in principle allows the calculation of the radiation power for particular solutions of the Nambu equations of motion. One important consequence of this formula is the fact that there is no contribution to the radiation power from the fundamental mode (n=1). (Note that the corresponding expressions for gravitational radiation power are given in Appendix C.)

Linearized radiation power expression

Unfortunately, it is still difficult in most cases to calculate the radiation power using (20). However, this expression can be linearized by considering only first order terms in the modulus of radial perturbations [Hina]. One infinite periodic solution of (17) and (18) is

$$X^{\mu} = (\tau, \mathbf{X}^{\perp}, \alpha\sigma + P_1(u) + P_2(v)). \tag{22}$$

In linearizing, we shall ignore powers of $|X^{\perp}|^2$ or greater. The actual radiation expressions previously derived for gravitational radiation are not correct. Here we deduce the analogous expression for Goldstone boson radiation from a global string, while the corrected result for gravitational radiation can be found in Appendix C.

The gauge constraints (15), in null worldsheet coordinates (u, v), can be written as

$$(\partial_u X^3)^2 + (\partial_u \mathbf{X}^\perp)^2 = \frac{1}{4}, \quad (\partial_v X^3)^2 + (\partial_v \mathbf{X}^\perp)^2 = \frac{1}{4}.$$
 (23)

Rearranging and using a Taylor series expansion gives

$$\partial_u X^3 \simeq \frac{1}{2} \left(1 - 2(\partial_u \mathbf{X}^\perp)^2 \right), \quad \partial_v X^3 \simeq \frac{1}{2} \left(1 - 2(\partial_v \mathbf{X}^\perp)^2 \right).$$
 (24)

Hence to first order, $X^3 = (u+v)/2$ so $\alpha = 1$, $P_1 = 0$ and $P_2 = 0$. We can write the linearized expression for X_R and X_L as

$$X_R^{\mu}(u) = \left(-\frac{1}{2}u, \mathbf{X}_R^{\perp}(u), \frac{1}{2}u\right) \quad X_L^{\mu}(v) = \left(\frac{1}{2}v, \mathbf{X}_L^{\perp}(v), \frac{1}{2}v\right).$$
 (25)

These expressions can be inserted into (21) for U^{μ} and V^{μ} . Integrating U^{0} , V^{0} , U^{3} and V^{3} by parts and linearizing the exponential then gives

$$U^{\mu} = \left(\frac{L}{2\pi(m+n)}\mathbf{k}^{\perp}.\mathbf{U}^{\perp}, \mathbf{U}^{\perp}, \frac{-L}{2\pi(m+n)}\mathbf{k}^{\perp}.\mathbf{U}^{\perp}\right),$$

$$V^{\mu} = \left(\frac{L}{2\pi(n-m)}\mathbf{k}^{\perp}.\mathbf{V}^{\perp}, \mathbf{V}^{\perp}, \frac{L}{2\pi(n-m)}\mathbf{k}^{\perp}.\mathbf{V}^{\perp}\right),$$
(26)

where

$$\mathbf{U}^{\perp} = \int_{0}^{L} \frac{du}{L} \partial_{u} \mathbf{X}_{R}^{\perp} e^{i\pi(m+n)u/L} ,$$

$$\mathbf{V}^{\perp} = \int_{0}^{L} \frac{dv}{L} \partial_{v} \mathbf{X}_{L}^{\perp} e^{i\pi(m-n)v/L} ,$$

$$\mathbf{k}^{\perp} = |\mathbf{k}^{\perp}| \hat{\mathbf{n}} = |\mathbf{k}^{\perp}| (\cos \varphi, \sin \varphi) .$$
(27)

Therefore, one can deduce expressions for $|U|^2$, $|V|^2$, $|U^*.V|$ and |U.V| in terms of the linearized variables \mathbf{U}^{\perp} , \mathbf{V}^{\perp} and $\hat{\mathbf{n}}$, that is,

$$|U|^{2} = -|\mathbf{U}^{\perp}|^{2}, \quad |V|^{2} = -|\mathbf{V}^{\perp}|^{2}$$

$$U^{*}.V = 2(\hat{\mathbf{n}}.\mathbf{U}^{\perp *})(\hat{\mathbf{n}}.\mathbf{V}^{\perp}) - \mathbf{U}^{\perp *}.\mathbf{V}^{\perp},$$

$$U.V = 2(\hat{\mathbf{n}}.\mathbf{U}^{\perp})(\hat{\mathbf{n}}.\mathbf{V}^{\perp}) - \mathbf{U}^{\perp}.\mathbf{V}^{\perp}.$$
(28)

We are now in a position to evaluate the φ -integration as the only remaining dependence is in $\hat{\mathbf{n}}$. The following formulae for $\mathbf{W}, \mathbf{X}, \mathbf{Y}, \mathbf{Z}$ (all two dimensional vectors) are easily obtained,

$$\int_{0}^{2\pi} d\varphi \left(\hat{\mathbf{n}}.\mathbf{X}\right) (\hat{\mathbf{n}}.\mathbf{Y}) = \pi \mathbf{X}.\mathbf{Y}$$
(29)

$$\int_{0}^{2\pi} d\varphi \left(\hat{\mathbf{n}}.\mathbf{W} \right) (\hat{\mathbf{n}}.\mathbf{X}) (\hat{\mathbf{n}}.\mathbf{Y}) (\hat{\mathbf{n}}.\mathbf{Z}) = \frac{\pi}{4} \bigg((\mathbf{W}.\mathbf{X}) (\mathbf{Y}.\mathbf{Z}) + (\mathbf{Z}.\mathbf{W}) (\mathbf{X}.\mathbf{Y}) + (\mathbf{X}.\mathbf{Z}) (\mathbf{W}.\mathbf{Y}) \bigg). \tag{30}$$

Applying these formulae to the power expression (20) with (28) yields

$$\frac{dP}{dz} = \frac{8\pi^3 f_a^2}{L} \sum_{n=1}^{\infty} n \sum_{\substack{|m| < n \\ m+n \text{ even}}} \left\{ |\mathbf{U}^{\perp}|^2 |\mathbf{V}^{\perp}|^2 + |\mathbf{U}^{\perp *} \cdot \mathbf{V}^{\perp}|^2 - |\mathbf{U}^{\perp} \cdot \mathbf{V}^{\perp}|^2 \right\}.$$
(31)

If one of the components of \mathbf{X}^{\perp} is zero then the linearized power expression can be simplified further

$$\frac{dP}{dz} = \frac{8\pi^3 f_a^2}{L} \sum_{n=1}^{\infty} n \sum_{\substack{|m| < n \\ m+n \text{ even}}} |\mathbf{U}^{\perp}|^2 |\mathbf{V}^{\perp}|^2.$$
 (32)

The linearized power expression (31) will only give the leading order term if the average value of $|\mathbf{X}^{\perp}|$ is sufficiently small, note also that it is possible that there is no contribution at this order. Note also from (20) or (31) that left-moving modes propagating along a straight string will not radiate if right-moving modes are absent (and vice versa).

Radiation power for specific solutions

Long string configurations can be quantified by the wavelength, λ (= L) and the amplitude, A. For solutions of the form (22), the important parameters are the ratio of the amplitude to wavelength, $\varepsilon = 2\pi A/\lambda$ (denoted the relative amplitude), and the oscillation frequency, $\Omega = 2\pi/\lambda$. In particular, we note that solutions for which $\varepsilon > 1$ are not allowed by (18) in our linearized description. Of course, solutions with $\varepsilon > 1$ are allowed for more general string configurations, but in the cases of high symmetry below they become highly degenerate with whole sections of string approaching luminal velocities (see the discussion in section 3).

Figure 2: Log-linear power spectrum of the helix solution at small ($\varepsilon = 0.2$) and large ($\varepsilon = 0.99$) amplitude.

(a) Helix solution

A simple, symmetric solution of the form (22) can be constructed from equal and oppositely propagating sine waves,

$$\mathbf{X} = \left(\frac{\varepsilon}{2\Omega} \left[\cos\Omega u + \cos\Omega v\right], \frac{\varepsilon}{2\Omega} \left[\sin\Omega u + \sin\Omega v\right], \frac{1}{2}\sqrt{1 - \varepsilon^2} \left(u + v\right)\right), \quad (33)$$

where $0 < \varepsilon < 1$ and $\varepsilon \to 1$ in the relativistic limit. This corresponds to a helicoidal solution which oscillates between a static helix and a straight line.

In this case we can use the full nonlinear analysis (20). The radiation power expression contains many Bessel functions with argument $\tilde{k} = \frac{1}{2}k\sqrt{n^2 - m^2/(1 - \varepsilon^2)}$,

$$\frac{dP}{dz} = \sum_{n=1}^{\infty} P_n = \sum_{n=1}^{\infty} \sum_{|m| < n\sqrt{1-\varepsilon^2}} \tilde{P}_{n,m}, \qquad (34)$$

where

$$\tilde{P}_{n,m} = \frac{\pi^2 \Omega f_a^2}{1 - \varepsilon^2} \left[-\frac{1}{4} \varepsilon^4 \left((J_l J_{u+1} - J_u J_{l+1})^2 + (J_u J_{l-1} - J_l J_{u-1})^2 - 2J_l^2 J_u^2 \right) \right.$$

$$\left. - \frac{1}{2} (J_{l+1} J_{u-1} - J_{l-1} J_{u+1})^2 + \varepsilon^2 J_l J_u (2J_l J_u - J_{l+1} J_{u-1} - J_{l-1} J_{u+1}) \right],$$

and

$$l = \frac{1}{2}(m+n), u = \frac{1}{2}(m-n).$$
 (36)

(This expression was previously obtained [Sakb], but without the shortcut provided by the left- and right-moving split of Appendix B.)

It can be easily shown that $\tilde{P}_{n,0} = 0$ for all positive integer n. From this and the conditions $|m| < n\sqrt{1-\varepsilon^2}$ and m+n even, one can deduce that the lowest even harmonic radiating is given by

$$n_{\text{even}} = \min \left\{ n : n > \frac{2}{\sqrt{1 - \varepsilon^2}}, n \text{ an even integer} \right\}$$
 (37),

and the lowest odd harmonic is given by

$$n_{\text{odd}} = \min\{n : n > \frac{1}{\sqrt{1-\varepsilon^2}}, \text{ } n \text{ an odd integer}\}$$
 (38)

For all ε , $n_{\rm even}$ is greater than two and, for $\varepsilon < \varepsilon_{\rm crit} = 0.94$, $n_{\rm odd}$ is three. Therefore for $\varepsilon < \varepsilon_{\rm crit}$, the third harmonic is the dominant contribution to the radiation power of the helix. In this case, one can deduce a linearized power expression by calculating the power in the third harmonic to first order in ε , which gives

$$\frac{dP}{dz} \simeq \frac{4\pi^3 f_a^2 \varepsilon^{10}}{125L}.\tag{39}$$

Applying the linearized power expression (31) to this solution gives zero, as it only takes into account terms of order ε^4 and below.

For $\varepsilon < \varepsilon_{\rm crit}$, one can see from fig. 2 that the power in the nth harmonic decays exponentially, with exponent proportional to n for large n (that is, $P_n \propto e^{-\alpha n}$, n >> 1). Fig. 3 illustrates how α varies with ε , showing that the exponential fall-off α becomes larger at small ε . The proposal of Sikvie et al. for radiation from long strings requires that $P_n \propto n^{-1}$. This contention should also be contrasted with the result for the Burden-Tassie loop solutions $(P_n \propto n^{-4/3})$ and kinky loops $(P_n \propto n^{-2})$ [VVa].

The helix solution has a great deal of symmetry which probably causes the cancellation of the second harmonic. Configurations of this type would not be expected to form in a realistic string network, because oppositely propagating modes will not have strong correlations. However, given that the helix is so weakly radiating, it conceivably could be the endpoint of a radiation process, say for small-scale structure on a large loop. The stability of this solution to radiation damping and other perturbations is, therefore, an interesting issue. Given that we do not observe the cancellation of the second harmonic in more general solutions, we believe that the helix is actually an exceptional result and will be unstable to stronger radiative decay (a contention for which we provide numerical evidence later). Nevertheless, it is not unreasonable to suggest that some helix properties, particularly the exponential fall-off of the harmonics at large n, will be generic for all $\varepsilon < 1$ long string solutions.

Figure 3: α against ε such that $P_n \propto e^{-\alpha n}$ for large n.

(b) Sine solution

A solution, similar to the helix, but with perturbations in only one direction is

$$\mathbf{X} = \left(\frac{\varepsilon}{2\Omega} \left[\cos \Omega u + \cos \Omega v\right], 0, \frac{1}{2\Omega} \left[E(\varepsilon, \Omega u) + E(\varepsilon, \Omega v)\right]\right),\tag{40}$$

where $E(k,\phi)$ is the incomplete elliptic integral of the second kind, defined by

$$E(k,\phi) = \int_0^\phi d\theta \sqrt{1 - \varepsilon^2 \sin^2 \theta}, \qquad (41)$$

where $0 < \varepsilon < 1$ and $\varepsilon \to 1$ in the relativistic limit.

The elliptic function can be written as a linearly increasing function plus a periodic function, so the solution can be seen to be in the form (22) and we can employ the power expressions (20) or (31). Unfortunately, the full nonlinear version (20) becomes too complicated, so we apply (31) to obtain

$$\frac{dP}{dz} = \frac{\pi^3 f_a^2 \varepsilon^4}{16L} \,. \tag{42}$$

This only yields the power up to order ε^4 , for which only contribution comes from the second harmonic (n=2). Presumably, as for the helix, the power will become dominated by higher order terms at large ε , but it seems reasonable to assume that

there also exists some $\varepsilon_{\text{crit}}$ below which (42) is a good approximation. In any case, for small amplitude waves it is clear that the dominant contribution to the radiation power comes from the second harmonic.

(c) Kink solution

It is well known that (18) has solutions with points at which the string velocity $\dot{\mathbf{x}}$ and tangent \mathbf{x}' are discontinuous; these points, known as kinks, propagate along the string at the speed of light. Here we give a simple solution for a periodic distribution of kinks on a long string, consisting of left and right moving perturbations, X_U and X_V respectively,

$$\mathbf{X} = \left(X_U + X_V, 0, \frac{1}{2}\sqrt{1 - \frac{4\varepsilon^2}{\pi^2}}(u+v)\right),\tag{43}$$

where

$$X_{U} = \begin{cases} \frac{2\varepsilon}{\pi} u & 0 < u < \frac{1}{4}L \\ \frac{2\varepsilon}{\pi} \left(\frac{1}{2}L - u\right) & \frac{1}{4}L < u < \frac{3}{4}L \\ \frac{2\varepsilon}{\pi} \left(-L + u\right) & \frac{3}{4}L < u < L \end{cases}, \tag{44}$$

$$X_{V} = \begin{cases} \frac{2\varepsilon}{\pi}v & 0 < v < \frac{1}{4}L\\ \frac{2\varepsilon}{\pi}\left(\frac{1}{2}L - v\right) & \frac{1}{4}L < v < \frac{3}{4}L\\ \frac{2\varepsilon}{\pi}\left(-L + v\right) & \frac{3}{4}L < v < L \end{cases}, \tag{45}$$

where $0 < \varepsilon < \frac{\pi}{2}$ and, in this case, $\varepsilon \to \frac{\pi}{2}$ is the relativistic limit.

Once more the full non-linear radiation power expression (20) is intractable, so we use the linearized version (31) which yields

$$\frac{dP}{dz} = \frac{8192 f_a^2 \varepsilon^4}{\pi^5 L} \sum_{n=1}^{\infty} n \sum_{\substack{|m| < n \\ m+n \text{ even}}} \frac{1}{(n^2 - m^2)^2} \left[1 - \cos \frac{\pi(m+n)}{2} \right] \left[1 - \cos \frac{\pi(m-n)}{2} \right]. \tag{46}$$

Again, this expression should be valid for $\varepsilon < \varepsilon_{\rm crit}$ for some $\varepsilon_{\rm crit}$, but even for sufficently small ε the radiation power is a logarithmically divergent infinite sum (that is, $P_n \propto n^{-1}$ for large n). This can be seen analytically from (46) since the sum is dominated by the m = n - 2 terms and numerically in fig. 4. The kink solution (43) is an infinite Fourier series over odd harmonics. However, in a physical context this divergence is cut off initially at the string width δ and at increasingly larger scales as radiation backreaction rapidly 'rounds' the kink. This 'rounding'

Figure 4: Log-log power spectrum for the kink solution showing power law fall-off.

will eliminate the more rapidly decaying high frequency contributions, ultimately leaving only the fundamental mode excitation.

(d) Spectrum of sinusoidal solutions

The following solution corresponds to a superposition of a large, but finite number, of sinusoidal perturbations,

$$\mathbf{X} = \left(\mathbf{X}^{\perp}, \sqrt{1 - \varepsilon^2}\right),\tag{47}$$

such that

$$\mathbf{X}^{\perp} = \frac{1}{2} \sum_{N \, st \, N \neq 0} \frac{\varepsilon}{N\Omega} \left[\mathbf{A}_N e^{iN\Omega u} + \mathbf{B}_N e^{iN\Omega v} \right], \tag{48}$$

where A_N and B_N satisfy

$$\mathbf{A}_{N}^{*} = -\mathbf{A}_{-N}, \quad \mathbf{B}_{N}^{*} = -\mathbf{B}_{-N},$$

$$\sum_{N \neq 0} |\mathbf{A}_{N}|^{2} = 1, \quad \sum_{N \neq 0} |\mathbf{B}_{N}|^{2} = 1,$$

$$\sum_{N \neq 0} \mathbf{A}_{N}.\mathbf{A}_{n-N} = 0, \quad \sum_{N \neq 0} \mathbf{B}_{N}.\mathbf{B}_{n-N} = 0 \quad \forall n \neq 0.$$
(49)

Such a random superposition more realistically models the perturbations expected on a string network. Using the linearized radiation power expression (31), we obtain

$$\frac{dP}{dz} = \frac{\pi^3 f_a^2 \varepsilon^4}{2L} \sum_{n=1}^{\infty} n \sum_{\substack{|m| < n \\ m+n \text{ even}}} \left[|\mathbf{A}_{\frac{m+n}{2}}|^2 |\mathbf{B}_{\frac{m-n}{2}}|^2 - |\mathbf{A}_{\frac{m+n}{2}} \cdot \mathbf{B}_{\frac{m-n}{2}}|^2 + |\mathbf{A}_{\frac{m+n}{2}}^* \cdot \mathbf{B}_{\frac{m-n}{2}}|^2 \right].$$
(50)

This illustrates the generic ε^4 dependence of the radiation power even for the higher oscillation frequencies. In special cases, such as the helix, the contribution at this order can cancel.

Simple backreaction model

The string configurations discussed in the previous section are solutions of the Nambu equations of motion. In flat space they will continue to oscillate forever at constant amplitude. Even in an expanding universe, the amplitude will only decay slightly due to Hubble damping once $\lambda < H^{-1}$. This is clearly physically unrealistic, as it takes no account of the fact that such configurations radiate Goldstone bosons. Here, we will endeavour to incorporate this radiation backreaction in some special cases.

In the previous section, we calculated the radiation power from several solutions, giving special consideration to the contribution from higher harmonics. This was only significant at large relative amplitude ε or for 'kinky' solutions. Even in these situations, however, our expectation is that these higher harmonics will be rapidly suppressed as their amplitude decays or the kink is rounded. Radiation power is soon dominated by one particular mode. For backreaction in this simple case, the expressions for the radiation power include powers of ε and one can deduce a phenomenological model for the decay of ε .

Given that the generic radiation power for any oscillation mode is proportional to ε^4 , we can model radiation damping by considering the following equations,*

$$E = \mu + \alpha \mu \varepsilon^{2} ,$$

$$\frac{dP}{dz} = -\frac{dE}{dt} = \frac{\beta \varepsilon^{4}}{L} ,$$
(51)

where E is the energy per unit length and α is the solution-dependent coefficient of ε^2 in the power series expansion of

$$\frac{1}{L} \int_0^L \frac{dX^3}{d\sigma} d\sigma \,. \tag{52}$$

^{*} Note we implicitly assume that the cut-off Δ for μ in (51) is comparable to the curvature radius of the oscillating string.

Figure 5: Oscillation energy against time For A=10, B=100 (unbroken line) and B=1000 (broken line).

For the sinusoidal solution $\alpha = \frac{1}{4}$, whereas for the helix $\alpha = \frac{1}{2}$ (as well as $\beta = 0$). In flat space, μ and L are constants so we can integrate the differential equation (51) to obtain

$$\varepsilon = \varepsilon_0 \left(1 + \frac{\beta \varepsilon_0^2}{\alpha \mu L} t \right)^{-1/2}, \quad E = \mu + \alpha \mu \varepsilon_0^2 \left(1 + \frac{\beta \varepsilon_0^2}{\alpha \mu L} t \right)^{-1}. \tag{53}$$

where initially $\varepsilon(0) = \varepsilon_0$. Defining $A = \mu$, $B = \alpha \mu \varepsilon_0^2$ and $C = \alpha \mu L/\beta \varepsilon_0^2$, this becomes

$$E = A + B\left(1 + \frac{t}{C}\right)^{-1}. (54)$$

Initially, the decay is linear (t << C), while asymptotically at late times (t >> C) the energy decays as a power law, t^{-1} . Fig. 5 shows the oscillation energy against time for some reasonable values of A, B and C. A useful property of the model is the effective half-life of the oscillation energy,

$$t_{1/2} = \alpha \mu L / \beta \varepsilon_0^2 \,. \tag{55}$$

The half-life depends on the initial relative amplitude ε_0 , increasing rapidly as ε_0 decreases.

The power law decay (54) of the oscillation energy provides a useful quantitative test of this formalism (see section 3), but it is a special case depending upon the left-and right-moving modes having equal amplitude. Strings in a realistic network will in general have a random superposition of unequal left- and right-moving modes. We can demonstrate heuristically that exponential decay will be generic for such modes. Suppose that ε_L and ε_R are the 'averaged' amplitudes of the left- and right-moving waves respectively. Motivated by (32) we might expect these modes to obey a cross-coupled version of (51) [Hinb], that is,

$$\alpha \mu \frac{d\varepsilon_R^2}{dt} = -\frac{\beta \varepsilon_L^2 \varepsilon_R^2}{L} \,, \quad \varepsilon_R(0) = A \,,$$

$$\alpha \mu \frac{d\varepsilon_L^2}{dt} = -\frac{\beta \varepsilon_L^2 \varepsilon_R^2}{L} \,, \quad \varepsilon_L(0) = B \,.$$
(56)

The solution we find in this case when $A \neq B$ is

$$\varepsilon_R^2 = \frac{A^2(B^2 - A^2)}{B^2 e^{\beta(B^2 - A^2)t/\alpha\mu L} - A^2},$$

$$\varepsilon_L^2 = \frac{B^2(B^2 - A^2)}{B^2 - A^2 e^{-\beta(B^2 - A^2)t/\alpha\mu L}},$$
(57)

The asymptotic behaviour of these solutions is of interest. In particular, we find that for B > A, $\varepsilon_R^2 \to 0$ and $\varepsilon_L^2 \to B^2 - A^2$ exponentially, whereas for B < A, $\varepsilon_L^2 \to 0$ and $\varepsilon_R^2 \to A^2 - B^2$. Whichever of the movers initially has the largest amplitude will approach a finite amplitude, while the other will decay to zero exponentially. The oscillation energy decay timescale again depends on the relative initial amplitudes.

3 Numerical methods and results

Algorithms and boundary conditions

As we have seen there is a duality between the Kalb-Ramond action (12) and the Goldstone action (4) in the presence of vortices. This duality implies that the two actions should exhibit the same dynamics. In the previous section the dynamics of various long string configurations were examined within the framework of the Kalb-Ramond action. Here we directly compare the results of simulations with the same configurations in the Goldstone model. We tackle this problem numerically because, as we have noted, the Goldstone action does not lend itself to simple analytic calculations due to the topological coupling of the massless field.

We have developed sophisticated numerical algorithms to allow the simulation of long string configurations within the framework of the Goldstone model. As in ref. [Sc], we discretize space on a three-dimensional grid with dimensions N_1, N_2, N_3 in the x, y, z directions respectively, solving the rescaled $(f_a \to 1, \lambda \to 2)$ Euler-Lagrange equation,

$$\frac{\partial^2 \Phi}{\partial t^2} - \frac{\partial^2 \Phi}{\partial x^2} - \frac{\partial^2 \Phi}{\partial y^2} - \frac{\partial^2 \Phi}{\partial z^2} + \Phi(\bar{\Phi}\Phi - 1) = 0.$$
 (58)

We employ a second-order leapfrog algorithm for the time derivative and second- or fourth-order finite difference approximations for the spatial derivatives (generally the latter). We denote the two algorithms as 2-2 and 2-4 respectively; they are discussed in greater detail elsewhere [BSa] (see also ref. [Sd]).

The cylindrically symmetric straight string ansatz (6) for the field requires that we solve the boundary value problem,

$$\frac{d^2\phi}{d^2r} + \frac{1}{r}\frac{d\phi}{dr} - \frac{1}{r^2}\phi - \phi(\phi^2 - 1) = 0,
\phi(r \to 0) = 0, \quad \phi(r \to \infty) = 1.$$
(59)

This was solved numerically using relaxation techniques. The finite boundary condition $\phi(r \to R) = 1$ introduces an error of order R^{-2} , which we minimize using a large grid and spatial step-size. We can perturb the straight string ansatz using the solutions defined in §2 with relative amplitude ε . We only impose perturbations in the x- and y-directions, thus introducing higher order errors, $\mathcal{O}(\varepsilon^2)$. However, these are negligible for small amplitude perturbations and so we effectively create highly accurate numerical solutions of the Nambu action.

It is appropriate at this point to comment on the string self-field and the radiation field since they are not easily distinguished in the Goldstone formalism. There are, however, particular configurations in which the two can be separated. For example, when a perturbed string straightens the massless self-field becomes azimuthal around the string as in (6) and the massive self-field can be easily calculated numerically from (59). In our simulations, this allows a straightforward subtraction at specified times to yield both the massless and massive radiation fields. Again, this procedure will be most accurate for small ε , though it still yields useful information for $\varepsilon \sim 1$.

Naturally the spatial discretization introduces boundaries into an otherwise unbounded problem. These artifical boundaries have an important effect on the numerical solution, especially at late times in problems involving radiation. For the long string configurations on the z-boundary we impose simple periodic, Dirichlet or Neumann boundary conditions. As in ref. [DSa], on the x- and y-boundaries we employ absorbing boundary conditions, except here using a higher-order second approximation version [EM] [EH] [BJR] (refer to ref. [BSa]). These absorbing boundary conditions require the solution of

$$\frac{\partial}{\partial t} \frac{\partial \Phi}{\partial x} - \frac{\partial^2 \Phi}{\partial t^2} + \frac{1}{2} \left(\frac{\partial^2 \Phi}{\partial t^2} + \frac{\partial^2 \Phi}{\partial t^2} \right) = 0, \tag{60}$$

at x = 0 and $x = N_1 \Delta x$ and a similar equation at y = 0 and $y = N_2 \Delta x$. These remarkable boundary conditions reflect a wave incident at 45° with only 3% of the original amplitude, that is, the reflected wave energy is reduced by a factor of 10^{-3} . Fig. 6 illustrates the efficacy of these boundary conditions by contrasting the absence of reflected radiation from absorbing boundary conditions with large reflections from Neumann boundary conditions for the same t. These allow the simulations to be evolved for many grid light-crossing times without significant influence on the

Figure 6: Comparison of (a) Neumann and (b) second approximation boundary conditions for typical string radiation at late times

interior string solution. Note that the grid face boundary conditions (60) must be appropriately augmented along the grid edges and at the corners [BSa].

Several runs were performed with Neumann boundary conditions on the xand y-boundaries to demonstrate energy conservation. Energy was conserved to
within 0.2% for both the 2-2 and 2-4 algorithms after several thousand timesteps.
Unfortunately, only first-order spatial differences were used in calculating the energy
density so no marked difference was evident between the two algorithms. We should
point out that the boundary conditions (60) only absorb massless radiation, but
strings emit both massless and massive radiation. The massive radiation in ϕ is not
easily excited and it is highly suppressed at small amplitude. Furthermore, because
of dispersion, it does not reach the boundary until late times. For reasonable values
of ε this massive radiation is barely detectable and has no discernible effect on string
motion.

We usually employed a grid with $N_1 = N_2 = 200$, $N_3 = 50$, and spatial and time step-sizes $\Delta x = 0.7$ and $\Delta t = 0.3$ (well within the Courant condition for these algorithms). Initial string configurations were demonstrated to be numerically stable for over 3000 timesteps, both in the interior and at the boundaries. The algorithm was used to study periodic helix, sine and kink long string solutions and circular loop collapse. Throughout the simulations we monitored the amplitude of the perturbed oscillation ε and the total energy per unit length E. We also analyzed the massless radiation spectrum using the three-dimensional spectral analysis techniques described in Appendix D.

Our numerical results will be seen to be at variance with those of Sikivie $et\ al.$ [HarS, HagS, Sikb] for three primary reasons:

(i) Firstly, in ref. [HagS] they analyzed the total massless field spectrum, including the string self-field, which introduces non-radiating higher harmonics into their spectral analysis. Fig. 7 demonstrates this clear difference between the total massless field spectrum and the radiation spectrum analysed after subtration of the string self-field. Notice that the self-field completely dominates the radiation field at this

Figure 7: Spectrum for (a) the total massless field (b) the radiation field

amplitude. Moreover, the fall-off in the higher modes for the total massless field spectrum is power-law $(P_n \propto n^{-1})$, whereas for the radiation spectrum it is much more rapid, being consistent with exponential.

(ii) Secondly, in ref. [HagS] they inadvertently concentrate on degenerate configurations with $\varepsilon > 1$ which do not correspond to the Nambu solutions presented in §2. These configurations are highly degenerate and collapse ultra-relativistically; whole regions along the string would achieve luminal velocities* but for radiation damping. An appropriate analogy is the perfectly circular loop solution which has a similar degeneracy and a corresponding pathological radiation divergence. Additional difficulties with these configurations are the inaccuracy of the ansatz (6) at large amplitude and the fact that our comparative analytic results only apply

^{*} These luminal string regions are known as 'lumps', and are distinct from 'cusps' where only a single string point reaches the speed of light. Unlike "lumps', cusps have a finite integrated radiation power [VVb].

Figure 8: Isosurfaces of the energy density for the evolving sine solution $(\varepsilon_0 = 0.6)$ shown after each period. Radiation damping causes a noticeable decrease in the oscillation amplitude.

in the ε < 1 regime. As it happens for small simulation scales, radiation damping for these "luminal" ε > 1 configurations is so effective that higher harmonics are only marginally more excited. Nevertheless, the ε > 1 results give the impression that the string is critically- or over-damped, whereas the ε < 1 configurations actually oscillate—as expected—like decaying Nambu solutions. In any case, such degenerate configurations would not be expected in a realistic string network, if only because of the presence of small-scale structure, and they are not, therefore, a reliable indicator of how it will radiate.

(iii) Thirdly, the reader is invited to compare the rather different spectral analysis methods of ref. [HagS] with those detailed in Appendix D. In particular, notice that the standard definition of the one sided three dimensional power spectrum (D3) and the related wave number (D2) are not used in ref. [HagS]. This apparent bin mislabelling will have an important effect on the numerically estimated power spectrum.

Massless radiation from the sine solution

The evolution of the sine perturbation (40) was simulated for a number of different initial amplitudes, ($\varepsilon_0 = 0.2, 0.3, ..., 1.2$) in order to obtain a quantative understanding of the evolution. As expected we find that the string oscillates losing amplitude by emitting radiation. Fig. 8 shows the decay of the maximum amplitude ε . Emitted radiation is illustrated in fig. 9 in a plane transverse to the string at the point of maximum amplitude. The radiation pattern is dominated by quadrupole lobes of the n = 2 harmonic.

We have analyzed the power spectra for $\varepsilon_0 = 0.4$, 0.6, 0.9; these are illustrated in fig. 10. The subtraction of the string self-field from the much smaller radiation field has to be performed precisely. Nevertheless, we found that some minor residuals could not be eliminated, notably in the third and fourth harmonics, because of the numerical inaccuracies inherent in this procedure and the nature of the ra-

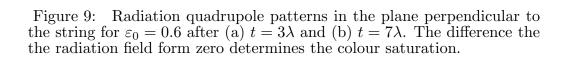


Figure 10: Radiation power spectrum for the sinusoidal solution on a log-linear scale for (a) $\varepsilon_0=0.4$, (b) $\varepsilon_0=0.6$ and (c) $\varepsilon_0=0.9$.

diation pattern near the string.* Configurations producing the strongest radiation provide the cleanest spectra ($\varepsilon_0 = 0.9$ in fig. 10c). We can only be confident that

^{*} These appear to be residuals because they remain when the oscillation energy

Figure 11: The contribution of the second fundamental mode to the radiation spectrum for $\varepsilon_0 = 0.6$.

these results provide an upper bound for the radiation in higher harmonics (n > 1), but we can still draw definite conclusions. First, it is clear that the lowest radiating harmonic (n=2) provides the dominant radiation component, as predicted analytically. Secondly, although some higher harmonics appear to be present, they are strongly suppressed by radiation into the lowest harmonic—even for $\varepsilon_0 \gtrsim 0.9$ they are not significantly excited. This is an important observation which confirms the assumption underlying our simple backreaction model in section 2. Finally, the decay in the higher harmonics is consistent, within the uncertainties, with an exponential fall-off. Without doubt it is completely inconsistent with a flat power law spectrum, $P_n \propto n^{-1}$. An n^{-1} fall-off would predict an amplitude for the n=10 harmonic relative to n=2 which is nine orders of magnitude larger than that observed in fig. 10c. The time evolution of the contribution to the radiation in the second harmonic is illustrated in fig. 11. The energy increases until the radiation propagates out to the edge of the box and begins to fall as the absorbing boundaries take effect.

and the n=2 radiation pattern have largely died away. We believe that they are due to an imperfect subtraction because the strings is not exactly straight at the discretized sampling timestep. The effect is also exacerbated by some distortion due to Lorentz contraction and the fact that the radiation pattern is only purely quadrupole asymptotically, not in the immediate vicinity of the oscillating string.

$arepsilon_0$	A	В	C
0.3	28.18	0.64	769.02
0.4	28.14	1.08	386.45
0.5	28.08	1.68	238.68
0.6	28.02	2.34	165.04
0.7	27.98	3.12	123.91
0.8	27.90	3.96	99.37
0.9	27.84	4.88	84.20
1.0	27.78	5.84	74.82
1.1	27.66	8.00	65.81
1.2	27.50	10.42	64.73

Table 1: Best fit values for the backreaction parameters A, B and C.

Figure 12: Energy against time: Numerical results and best fit curves for (a) $\varepsilon_0=0.5$, (b) $\varepsilon_0=0.8$ and (c) $\varepsilon_0=1.1$.

Evidence for quantitative agreement with the analytic radiation calculations comes from attempts to fit the time history of the overall energy density to the simple backreaction model (53). The total energy initially remains constant until the radiation propagates out to the boundary. At this stage it begins to fall with a time-delayed profile similar to that of our simple model. The least squares estimators for A, B and C in (54) are calculated using a global minimisation routine and are displayed in Table 1 for a variety of initial amplitudes.

We find that A is constant to within a few percent and the calculated values for B and C are in good agreement for $\varepsilon_0 \lesssim 1.1$. The numerical results and the best fit curves are shown in fig. 12 for $\varepsilon_0 = 0.5, 0.8, 1.1$. A more significant test comes from determining the dependence of B and C on ε_0 . This is shown in fig. 13 in a log-log plot, the points are well-fitted by a straight line in the region $0.3 \lesssim \varepsilon_0 \lesssim 0.8$. If we assume that $A = A_0$, $B = B_0 \varepsilon_0^{n_1}$ and $C = C_0 \varepsilon_0^{n_2}$ then we calculate least squares estimators, $A_0 = 28.0 \pm 0.4$, $\log B_0 = 1.7 \pm 0.2$, $\log C_0 = 4.2 \pm 0.4$, $n_1 = 2.0 \pm 0.1$ and $n_2 = -2.0 \pm 0.1$. These exponents are in excellent agreement with the predictions of the backreaction model (54). From these values we can obtain the parameters in (51), $\alpha = 0.2 \pm 0.05$ and $\beta = 3.5 \pm 1.75$. Given the uncertainties, these are again in satisfactory agreement with the actual analytic values, $\alpha = 0.25$ and $\beta = 1.98$ from (42). We can also calculate the value of the unrenormalized string tension by summing the massive field contributions to the energy of a straight string solution, yielding $\mu_0 = 4.2 \pm 0.2$. This allows us to estimate $\log(\Delta/\delta) = 3.8 \pm 0.2$. This indicates that the simulated global strings have approximately six times more energy in the Goldstone field than in the massive string core. These results, therefore, test and confirm the renormalization procedure which underlies the previous analytic predictions.

We have also numerically studied the dynamics and radiation spectra of sinusoidal solutions for $\varepsilon_0 > 1$ where the analytic results are invalid. These solutions are highly degenerate and were expected to produce a large amount of radiation in higher radiation modes, however, this was not found to be the case. Fig. 14 shows the radiation spectrum for $\varepsilon_0 = 2.0$, showing that the string predominantly radiates in the second harmonic even at these large amplitudes. This result indicates that radiation backreaction damps the excitation of higher harmonics much more strongly than expected. On these small simulation scales, massive radiation is also excited at large amplitude (see below) and this may contribute to the radiation damping.

Finally, we should comment on the related helix solution which is predicted to radiate extremely weakly (39). Interestingly, we observe that the helix appears to be dynamically unstable and radiates in a similar manner to the sine solution (mainly in the n=2 harmonic). This may be because our initial ansatz is not a sufficiently perfect representation of the true solution. However, we believe that the non-radiating property of the helix is a finely balanced result of its symmetry. Any asymmetry introduced by radiation damping or otherwise will tend to destabilize the solution towards others which generically radiate more strongly. This conjecture remains to be justified analytically.

Figure 13: Loglog plots of (a) B agianst ε_0 and (b) C against ε_0 .

Massless radiation from the kink solution

We have also studied the evolution of the kink solution (43) for a number of different initial perturbation amplitudes. In section 2 we proposed that the kink solution should radiate with an n^{-1} spectrum, truncated at some time-dependent 'rounding' scale. The effectiveness of this 'rounding' can be seen in fig. 15 which shows an initial kink perturbation evolving into a sinusoidal perturbation. The decay of high harmonics in the kink spectrum takes place very rapidly. Fig. 16 shows the radiation spectrum at early times (a), contrasted with the spectrum from late times (b). Note that the kink solution initially has more power in higher frequency radiation modes with a slow power law fall-off. The later spectrum (fig. 16b), however, is indistinguishable from a typical sinusoidal spectrum. These results certainly support our intuitive understanding of kink 'rounding'.

Massive radiation

We have already noted that global strings can radiate massive particles, as well as massless particles. Depending on the final decay products, massive radiation

Figure 14: The radiation spectrum for a large amplitude sine solution with $\varepsilon_0 = 2.0$. Notice the power in the higher harmonics which shows up in the log-linear spectrum.

from topological defects is of considerable interest because it has been proposed as a potential source of baryon asymmetry. Massive modes will be suppressed except in regions of high curvature, such as cusps and sharp kinks. In our simulations because the curvature radius is not much larger than the string width, massive radiation could be excited for large amplitude sinusoidal solutions, that is, $\varepsilon_0 \gtrsim 0.6$. Massive radiation produced by global strings exhibits very different behaviour to massless radiation. Fig. 17 illustrates a circular pattern reminiscent of dipole radiation, quite unlike the quadrupole patterns of fig. 9. As the string oscillates, massive radiation is emitted most strongly in the direction of string motion. However, note that for amplitudes below $\epsilon_0 < 0.9$ the massive radiation signal was relatively very weak. Massive radiation will be discussed in greater detail elsewhere [BSa].

Loop solutions

The radiation spectrum from oscillating loops was not easily accessible to nu-

Figure 15: Energy density isosurfaces for the kink solution ($\varepsilon_0 = 0.6$) shown after each period of its evolution. Note the effectiveness of 'rounding' due to radiation damping.

merical simulation because on these small scales radiation damping leads to their rapid demise. There are further numerical difficulties setting up appropriate initial configurations and distinguishing the radiation field from the loop self-field. Nevertheless, we illustrate the collapse of a perfectly circular loop in fig. 18. The loop begins to shrink rapidly under its own tension, and annihilation occurs when the opposite segments collide. At this stage massive radiation is also produced copiously. The massless radiation pattern after collapse is shown in fig. 19. The fact that the radiation is maximal in a direction transverse to the loop plane is consistent with analytic calculations for the circular solution. The predicted divergence in the the integrated power is, of course, removed by radiation backreaction and finite width effects. We note that this very degenerate loop configuration is expected to produce an atypical n^{-1} power spectrum, so we cannot infer general conclusions for loop radiation from this special case (as in ref. [HagS]).

Our expectation on cosmological scales for non-intersecting loop solutions is that the antisymmetric tensor formalism of ref. [VVa] will provide an accurate picture of loop radiation, that is generically $P_n \propto n^{-\alpha}$ with $\alpha \geq 3/2$ for n >> 1. In the final stages of loop decay when its radius approaches the core width, the demise will proceed more rapidly through annihilation as in fig. 18. The resulting small burst of massive radiation may have significant cosmological implications.

4 Discussion and conclusions

The conclusions of this work are unambiguous. We have made careful comparisons between high precision numerical simulations of the Goldstone model (4) with analytic calculations using the antisymmetric tensor formalism of the Kalb-Ramond action (12). The description of vortex-line dynamics with both approaches is found to be in close quantitative agreement. This has a number of important implica-

Figure 16: The radiation spectra for the kink solution after (a) $t = 3\lambda$ and (b) $t = 15\lambda$. Compare the latter with the sinusoidal spectrum given in fig. 7b.

tions, not least because the validity and usefulness of this duality had previously been questioned.

Firstly, this work confirms the procedure employed for passing between the Goldstone boson field ϑ and the antisymmetric tensor field $B^{\mu\nu}$ in the presence of vortices. Note that on the relatively small scales we consider in these simulations, the duality is not straightforward because the relation (8) is complicated by the behaviour of the massive field ϕ in the string core. Provided perturbation wavelengths are large compared to the string core width δ , we can integrate out the massive degrees of freedom to obtain the Nambu term in (12). Of course, for very high energy perturbations it proved possible to excite these internal massive degrees of freedom.

Secondly, the Nambu-like behaviour predicted for global strings in (16) depends upon the renormalization of the string self-field. (This is distinct from renormalization about a point source because it involves cut-offs at both small and large scales.) In our numerical simulations, we typically had an energy in the string self-field (the Goldstone mode) which exceeded that in the core (the massive mode) by a factor of about six. Nevertheless, but for radiative damping, the evolution of initially perturbed solutions was observed to closely correspond to oscillatory Nambu

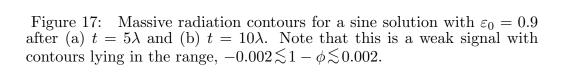


Figure 18: Energy density isosurfaces for a collapsing circular loop shown at intervals of 20 timesteps.

trajectories. In no sense is this self-field a diffuse 'cloud of energy' somehow distinct from the global string core. On the contrary, it is tightly bound to the string—the nearer the core, the more tightly. On scales below the string curvature radius, these massless modes merely renormalize (and dominate) the string tension and energy

Figure 19: Massless radiation contours in the aftermath of circular loop annihilation. Illustrated is a slice transvere to the plane in which the loop collapsed; very little radiation is emitted in the loop plane.

density.

Thirdly, as predicted by the Kalb-Ramond action, global strings radiate with a classical spectrum in harmonics directly related to the wavelengths of perturbations on the string. For example, for the sine solution we confirmed the absence of the fundamental mode, demonstrating that radiation was primarily in the second harmonic. This discrete spectrum appeared to be consistent with exponential fall-off at high harmonics for the long string configurations we studied, in complete contrast to the prediction of power law fall-off, $P_n \propto n^{-1}$, suggested in [HarS,HagS,Sikb]. Sharp kink configurations initially showed additional power for large n, but this was rapidly eliminated by rounding due to radiation damping, and the spectrum soon conformed to that for simple sine solutions.

Finally, we have numerically confirmed the quantitative rate of radiative backreaction predicted for particular long string configurations. Both the amplitude and decay rate of the oscillations on the strings were found to be in good agreement with our analytic results. Moreover, we observed that radiation damping was very effective at eliminating higher harmonics n > 2, markedly increasing the amplitude range over which our simple backreaction model gave satisfactory results. We are currently applying this work to more general string configurations because it has important implications for the understanding of string network evolution and, specifically, the build-up and damping of small-scale structure on strings. Modifications to (16) and direct comparisons with field theory simulations are the subject of a forthcoming publication [BSb].

It is interesting to place these results in a cosmological context because this formed our initial motivation. For heavy cosmological strings, the logarithm in $\mu(\Delta)$ is much larger $(\ln(\Delta/\delta) \sim 70\text{--}100)$ than for strings in our simulations. Although the emitted power remains the same, the overall decay rate is slower because the radiation damping term in (16) is relatively weaker. Conversely, however, these strings can be expected to produce more radiation in higher harmonics because the string trajectory will more nearly approach the strongly radiating configurations

allowed by the Nambu equations, notably cusps.

We believe that these results leave little doubt that the low-energy effective Kalb-Ramond action provides an excellent quantitative description of global string dynamics and radiation. Of course, as we have observed with massive excitations, the antisymmetric tensor description needs to be supplemented with the full nonlinear field theory in very high curvature regions, such as at points of string intersection or cusps. However, these regions typically have length-scales corresponding to the string core width δ , so in a macroscopic context they will have a very minor effect on overall predictions of massless radiation. In cosmology these results imply that the antisymmetric tensor formalism should provide an accurate picture of axion production by an axion string network as described in ref. [VVa, DSa, Sakb], but contrary to the assertions of refs. [HarS, HaqS, Sikb]. Whether or not this has been achieved with sufficient precision at this stage remains an open question which we briefly take up in Appendix A. However, axion strings are by no means the only application of this elegant and tractable formalism; global strings also appear in low-temperature and other contexts. Indeed, refs. [DSc, GKPB] demonstrated the close relationship between global strings in the Goldstone model (4) and vortex-lines in a 'relativistic' superfluid. In ref. [Car] this has been generalized to compressible superfluids and perfect fluids, so it may be that the methods described here—both analytic and numerical—can be usefully applied and tested in a laboratory setting.

Acknowledgements

We have benefitted from useful discussions with Mark Hindmarsh. We are also grateful for conversations with Brad Baxter, Brandon Carter and Mary Sakellariodou. We both acknowledge the support of the Science and Engineering Research Council, including the Cambridge Relativity group rolling grant (GR/H71550) and Computational Science Initiative grants (GR/H67652 & GR/H57585).

Appendix A: Axion string bounds revisited

The astrophysical and cosmological constraints on the axion were introduced in section 1. Here we consider the axion string bound in the light of our previous discussions, specifically noting the relative axion contributions radiated by small loops and long strings. Of course, we assume the standard axion scenario with the universe passing through the Peccei-Quinn phase transition after reheating.

Cosmic string evolution in an expanding universe has been extensively studied numerically [AT,BB,AShe]. A long string network loses energy through loop production and is observed to evolve toward a 'scaling' regime in which its large-scale properties remain constant relative to the horizon. These robust large-scale results were obtained for local gauge strings but they can also be expected to apply to global strings. The overall long-string energy density, however, must be modified with a logarithmic time dependence arising through the cutoff $(\Delta \sim t)$ in the global string energy density μ , that is,

$$\rho_{\infty} = \frac{\zeta \mu}{t^2} \approx \frac{2\pi \zeta f_{\rm a}^2}{t^2} \ln(t/\delta) \,, \tag{A1}$$

where $\zeta \approx 14$ [BB,AShe]. The network correlation length is then given approximately by $\xi = \zeta^{-1/2}t$.

In numerical simulations, evolution on small scales does not actually 'scale', though this appears to have little effect on the overall density (A1) and correlation length ξ . In any case, in a realistic setting, this small-scale structure will be limited by radiation backreaction, damping out perturbations below a constant relative scale, $L_r \equiv \kappa t$. The long-string backreaction scale L_r should provide an lower limit to the typical 'scaling' size of loops created by the network, $\ell = \alpha t$.

Axions will be radiated by loops and long strings until the axion mass 'switches on' at the time $t_{\rm w}=t_{\rm QCD}$ when domain walls form, causing the rapid demise of the network. We can provide a greatly simplified estimate of the resulting number density of axions n_a by noting that the dominant contribution comes from the least relativistic axions created just before $t_{\rm QCD}$ [Davb] (refer to ref. [VS]). To maintain scaling in each Hubble time, the long-string network must lose most of its energy to loops which, in turn, rapidly decay into axions of roughly the same wavelength. Just prior to $t_{\rm w}$, then, loops will have made the following contribution to the axion energy density,

$$\rho_{a\ell} \approx \frac{2\pi \zeta f_a^2}{t_w^2} \ln(t_w/\delta) \,. \tag{A2}$$

These axions will typically have a frequency, $\omega = 4\pi/\alpha t$, because loops of length $\ell \approx \alpha t$ radiate primarily in their fundamental mode $2/\ell$. For massless axions we have $\rho_{\rm a} = n_{\rm a}\omega$, so the number density of axions remaining at $t_{\rm w}$ is approximately

$$n_{\rm a\,\ell} \approx \frac{\alpha \zeta f_{\rm a}^2}{2t_{\rm w}} \ln(t_{\rm w}/\delta) \,.$$
 (A3)

Clearly, a determination of the loop-size parameter α is essential for a quantitative estimate of the axion density today.

Loop creation will occur on scales limited by the long-string radiation back-reaction scale, that is, $\alpha \gtrsim \kappa$. Recalling the damping 'half-life' $t_{1/2} = \alpha' \mu L/\beta \varepsilon_0^2$ defined in section 2, we can determine the minimum length-scale $L \approx \kappa t$ which will have lost most of its energy in one Hubble time:

$$\kappa \sim \frac{\pi^2}{8} \left[\ln(t/\delta) \right]^{-1} \,, \tag{A4}$$

where we have taken $\beta = \pi^3 f_{\rm a}^2/16$ and $\alpha' = 0.25$ for the sine solution (47), while also assuming $\varepsilon_0 \approx 1$. This yields $\kappa \sim 0.02$ at $t_{\rm QCD}$, but large uncertainties must be admitted. It seems reasonable, therefore, along with previous authors to take $\alpha \sim 0.1 \ [VVa, VS]$.

By equal matter-radiation $t_{\rm eq}$, the now-massive axions in (A3) are non-relativistic, so the axion density is given simply by $\rho_{\rm a} \approx m_{\rm a} n_{\rm a}$, where $n_{\rm a}$ has been appropriately diluted by the expansion a^{-3} . A comparison at $t_{\rm eq}$ between $\rho_{\rm a}$ and the critical density $\rho_{\rm c}$ yields the cosmological constraints [VS],

$$m_{\rm a} \gtrsim 10^{-4} \,\text{eV} \,, \qquad f_{\rm a} \lesssim 10^{11} \,\text{GeV} \,,$$
 (A5)

where we have assumed $\alpha \sim 0.1$.

A rough estimate of the axion contribution from long string radiation is also straightforward. According to (42), the power radiated per unit length is given by

$$\frac{dP}{dz} = \frac{\pi^3 f_{\rm a}^2}{16\gamma t} \,,\tag{A6}$$

where we assume perturbations are peaked at some length-scale γt ($\kappa < \gamma < \zeta^{-1/2}$), for which the relative amplitude $\varepsilon \approx 1$. We now multiply by t and the total length of string ζ/t^2 to obtain the axion energy density radiated in one Hubble time prior to $t_{\rm w}$,

$$\rho_{\rm a\,\infty} \approx \frac{\pi^3 \zeta f_{\rm a}^2}{16\gamma t_{\rm w}^2} \,. \tag{A7}$$

Given radiation in the second harmonic $\omega = 4\pi/\gamma t$, we obtain the long string axion number density

$$n_{\rm a\,\infty} \approx \frac{\pi^2 \zeta f_{\rm a}^2}{64t_{\rm w}} \,. \tag{A8}$$

Note that the axion (or graviton etc.) number radiated by long strings appears to be independent of the actual perturbation length-scale which dominates the spectrum.

A comparison between contributions from loops (A3) and long strings (A8), yields the relative density ratio

$$\frac{\Omega_{\rm a\,\ell}}{\Omega_{\rm a\,\infty}} \approx \frac{32\alpha}{\pi^2} \ln(t_{\rm w}/\delta) \approx \frac{4\alpha}{\kappa} \,.$$
 (A9)

If loops are created above the backreaction scale $\alpha \gtrsim \kappa$, then the axion density produced by long strings is probably subdominant. However, if $\alpha \sim \kappa$ these densities may be comparable. As mentioned in section 1, there are also other sources such as axion emission during domain wall decay. Again, approximate estimates suggest that this contribution cannot be neglected in determining a final cosmological bound on the axion [Lyta].

It remains to comment on the axion string constraints presented in earlier work. It is apparent that the bound (5) is weaker than the original string bound (3), $f_a \lesssim 10^{10} \text{GeV}$, of refs. [Davb,DSa]. The difference lies not in the understanding of global string radiation—which agrees with this analysis—but, rather, in whether the dominant network energy loss comes from small loop creation or long string radiation. The assumption [Dava] that it comes from long strings radiating at the correlation length $\xi \approx t$ seems to give an order-of-magnitude overestimate (comparable to taking the loop result (A3) with $\alpha \approx 1$). The apparent severity of this old long string constraint is illustrated in fig. 20.

The difference between (A5) and the string bounds of refs. [HarS,HagS,Sikb] are more fundamental because they are based on the assumption that global strings radiate with a flat power spectrum, $P_n \propto n^{-1}$. This is contrary to our results which show that power is generally dominated by the lowest allowed harmonic. The remaining literature on cosmological axion constraints has been flawed either

Figure 20: Schematic of the approximate astrophysical and cosmological bounds on the axion. The viability of the axion in the standard scenario clearly depends on an improved understanding of axion string radiation. The conclusions of this paper indicate that the true constraint will lie somewhere near the string loop bound (5), leaving a a somewhat smaller—but still substantial—parameter window.

by prevarication on this issue or by ignoring topological effects altogether. Authors have preferred to reserve judgment on the underlying global string spectrum, while discussing the consequences of both alternatives (see, for example, refs. [Lyta, KT]).

This paper only constitutes a first step towards a definitive axion string constraint. While it supports the assumptions on which (A5) is based, we make no suggestion that axion detection experiments should either be launched or cancelled on the basis of the uncertain parameter window shown in fig. 20. However, we do hope to remove these remaining uncertainties with large-scale string network simulations which incorporate radiation backreaction.

Appendix B: Power expression split with left- and right-movers

One can split arbitrary solutions of the Nambu equations into left- and right-moving waves by employing null coordinates on the string worldsheet $u = \sigma - \tau$ and $v = \sigma - \tau$ (ie. $X^{\mu} = X_R^{\mu} + X_L^{\mu}$). This was first used by Burden [Bur] to separate the Fourier transform of the energy-momentum tensor into left- and right-moving

components when calculating the gravitational radiation power from a closed loop (see a more extensive discussion in [AShe2]). This split has also been performed for a long periodic string [Hina]; unfortunately, however, there was a slight oversight which has important consequences for the allowed spectrum of radiation.

Here we outline the left- and right-splitting of the Fourier transform of the source distribution $\widetilde{J}^{\mu\nu}$ for a z-directed long global string, periodic in σ and τ with period L and $X^3 = \alpha \sigma$ (conditions satisfied by the helix solution (33)). We then discuss the generalization to the case where $X^3 = \alpha \sigma + P_1(u) + P_2(v)$ such that P_1 and P_2 are arbitrary (small) functions with period L. In the special case of $X^3 = \alpha \sigma$, we have

$$J^{\mu\nu}(\mathbf{x}^{\perp}, z, t) = \frac{f_a}{2} \int_{-\infty}^{\infty} d\sigma \int_{-\infty}^{\infty} d\tau (\dot{X}^{\mu} X^{\prime\nu} - X^{\prime\mu} \dot{X}^{\nu}) \times \delta^{2}(\mathbf{x}^{\perp} - \mathbf{X}) \delta(z - \alpha\sigma) \delta(t - \tau) ,$$

$$\widetilde{J}^{\mu\nu}(\mathbf{k}^{\perp}, \kappa_{m}, \omega_{n}) = \frac{1}{\alpha L^{2}} \int_{0}^{L} dt \int_{0}^{\alpha L} dz \int d^{2}\mathbf{x}^{\perp} J^{\mu\nu}(\mathbf{x}^{\perp}, z, t) e^{-ik.X} ,$$
(B1)

for $n \neq 0$ and $k^{\mu} = (\mathbf{k}^{\perp}, \kappa_m, \omega_n)$ where $\omega_n = 2\pi n/L$, $\kappa_m = 2\pi m/\alpha L$. Using these definitions one can deduce that

$$\widetilde{J}^{\mu\nu}(\mathbf{k}^{\perp}, \kappa_m, \omega_n) = \frac{f_a}{2\alpha l^2} \int_0^L d\sigma \int_0^L d\tau (\dot{X}^{\mu} X^{\prime\nu} - X^{\prime\mu} \dot{X}^{\nu}) e^{-ikX} ,
\equiv \int_0^L d\sigma \int_0^L d\tau I .$$
(B2)

We now change the variables of integration from (σ, τ) to the null coordinates (u, v), in which I can be re-expressed as

$$\dot{X}^{\mu}X^{\prime\nu} - X^{\prime\mu}\dot{X}^{\nu} = 2\left(\partial_{v}X_{L}^{\nu}\partial_{u}X_{R}^{\mu} - \partial_{u}X_{R}^{\mu}\partial_{v}X_{L}^{\nu}\right). \tag{B3}$$

The region of integration is more complicated. Fig. 21 shows how the integration over the region $0 < \sigma < L$ and $0 < \tau < L$ (that is, $R_1 \cup R_2 \cup R_3 \cup R_4$) can be transformed into an integration over the region 0 < u < L and 0 < v < 2L ($R_1 \cup R_2' \cup R_3' \cup R_4$). This can be further simplified by noting that

$$\int_{R_4 \cup R_2'} du dv I = e^{i(m+n)\pi} \int_{R_1 \cup R_3'} du dv I$$
 (B4)

Therefore we can write the Fourier transform of the source distribution function in terms of left- and right-movers as

$$\widetilde{J}^{\mu\nu}(\mathbf{k}^{\perp}, \kappa_m, \omega_n) = \frac{f_a}{\alpha} \left[U^{\mu} V^{\nu} - V^{\mu} U^{\nu} \right]$$
 (B5)

Figure 21: Equivalent regions of integration for (σ, τ) and (u, v).

where

$$U^{\mu} = \int_{0}^{L} \frac{du}{L} \partial_{u} X_{R}^{\mu} e^{-ik.X_{R}(u)},$$

$$V^{\mu} = \int_{0}^{L} \frac{dv}{L} \partial_{v} X_{L}^{\mu} e^{-ik.X_{L}(v)},$$

$$k^{\mu} = (\omega_{n}, \mathbf{k}^{\perp}, \kappa_{m}).$$
(B6)

where m + n must be even. This condition was missed in the previous derivation and has a important effect on the allowed spectrum of radiation. In particular it is responsible for there being no contribution from the fundamental harmonic (n=1).

The generalisation of this splitting to a solution with $X^3 = \alpha \sigma + P_1(u) + P_2(v)$ can be achieved, assuming the P_1 and P_2 are sufficiently small by allowing the lines bounding the regions R_1, R_2, R_3 and R_4 to become oscillatory. The periodicity of fig. 21 is maintained by the periodicity of P_1 and P_2 .

Appendix C: Formulae for gravitational radiation power

This appendix gives gravitational radiation power expressions for local strings, analogous to the those for Goldstone bosons from global strings. The source term for the gravitational radiation is the energy—momentum tensor

$$T^{\mu\nu} = \mu_0 \int (\dot{X}^{\mu} \dot{X}^{\nu} - X'^{\mu} X'^{\nu}) \delta^{(4)}[x - X(\sigma, \tau)] \, d\sigma d\tau \,, \tag{C1}$$

and the radiation power is given by

$$\frac{dP}{dz} = 2G \sum_{n=1}^{\infty} \omega_n \sum_{m \, st \, |\kappa_m| < \alpha \omega_n} \int_0^{2\pi} d\varphi \left(\widetilde{T}^{\mu\nu*}(\omega_n, \mathbf{k}^{\perp}, \kappa_m) \, \widetilde{T}_{\mu\nu}(\omega_n, \mathbf{k}^{\perp}, \kappa_m) \right) - \frac{1}{2} |T_{\lambda}^{\lambda}(\omega_n, \mathbf{k}^{\perp}, \kappa_m)|^2 \right).$$
(C2)

On performing the split into left- and right-movers, as in appendix B, one can deduce that

$$\frac{dP}{dz} = \frac{32\pi G\mu_0^2}{\alpha^2 L} \sum_{n=1}^{\infty} n \sum_{\substack{|m| < \alpha n \\ m+n \text{ even}}} \int_0^{2\pi} d\varphi \{|U|^2 |V|^2 + |U^* \cdot V|^2 - |U \cdot V|^2\},$$
 (C3)

and the corresponding linearized power expression is given by

$$\frac{dP}{dz} = \frac{64\pi G\mu_0^2}{L} \sum_{n=1}^{\infty} n \sum_{\substack{|m| < n \\ m+n \text{ even}}} \left\{ |\mathbf{U}^{\perp}|^2 |\mathbf{V}^{\perp}|^2 - |\mathbf{U}^{\perp *} \cdot \mathbf{V}^{\perp}|^2 + |\mathbf{U}^{\perp} \cdot \mathbf{V}^{\perp}|^2 \right\}.$$
 (C4)

Note the difference between the previous expression (C3) and the linearized version (C4) (a correction for ref. [Hina]). Applying (C4) to the helix, sine, kink and sine spectrum solutions discussed in section 2 yields the following

Helix:
$$\frac{dP}{dz} = \frac{4\pi^2 G \mu_0^2 \varepsilon^4}{L},$$

$$dP = \pi^2 G \mu_0^2 \varepsilon^4$$
(C5)

Sine:
$$\frac{dP}{dz} = \frac{\pi^2 G \mu_0^2 \varepsilon^4}{2L} \,, \tag{C6}$$

Kink:
$$\frac{dP}{dz} = \frac{65536G\mu_0^2 \varepsilon^4}{\pi^6 L} \sum_{n=1}^{\infty} n \sum_{\substack{|m| < n \\ m+n \text{ even}}} \frac{1}{(n^2 - m^2)^2},$$

$$\times \left[1 - \cos\frac{\pi(m+n)}{2}\right] \left[1 - \cos\frac{\pi(m-n)}{2}\right], \quad (C7)$$

Sine spectrum:
$$\frac{dP}{dz} = \frac{4\pi^2 G \mu_0^2 \varepsilon^4}{L} \sum_{n=1}^{\infty} \sum_{\substack{|m| < n \\ m+n \text{ even}}} \left[|\mathbf{A}_{\frac{m+n}{2}}|^2 |\mathbf{B}_{\frac{m-n}{2}}|^2 \right]$$

$$+ |\mathbf{A}_{\frac{m+n}{2}}.\mathbf{B}_{\frac{m-n}{2}}|^2 - |\mathbf{A}_{\frac{m+n}{2}}^*.\mathbf{B}_{\frac{m-n}{2}}|^2$$
 (C8)

This behaviour is very similar to antisymmetric tensor radiation. The notable exception is the helix solution which radiates gravitationally in the second harmonic, underlining the incongruous nature of the Goldstone boson result. Note also that the linearized power expressions above are only valid for $\varepsilon < \varepsilon_{\text{crit}}$ for some $\varepsilon_{\text{crit}} = \mathcal{O}(1)$. A simple backreaction model for gravitational radiation will take the same form as (54).

Appendix D: Three-dimensional spectral analysis

Standard methods for power spectrum analysis [W,H,M] are applied to the radiation field on a three-dimensional grid. This involves calculation of the three-dimensional discrete Fourier transform using an FFT algorithm. The three-dimensional Fourier transform, $\widetilde{F}_{\beta_1,\beta_2,\beta_3}$, of some discrete function $F_{\alpha_1,\alpha_2,\alpha_3}$ is given by

$$\widetilde{F}_{\beta_1,\beta_2,\beta_3} = \frac{1}{\sqrt{N_1 N_2 N_3}} \sum_{\alpha_1=1}^{N_1-1} \sum_{\alpha_2=1}^{N_2-1} \sum_{\alpha_3=1}^{N_3-1} F_{\alpha_1,\alpha_2,\alpha_3} e^{-2i\pi \left(\frac{\alpha_1 \beta_1}{N_1} + \frac{\alpha_2 \beta_2}{N_2} + \frac{\alpha_3 \beta_3}{N_3}\right)}, \quad (D1)$$

where

$$F_{\alpha_{1},\alpha_{2},\alpha_{3}} \simeq F(\alpha_{1}\Delta x, \alpha_{2}\Delta y, \alpha_{3}\Delta z),$$

$$\widetilde{F}_{\beta_{1},\beta_{2},\beta_{3}} \simeq \widetilde{F}\left(\frac{2\pi\beta_{1}}{N_{1}\Delta x}, \frac{2\pi\beta_{2}}{N_{2}\Delta x}, \frac{2\pi\beta_{2}}{N_{3}\Delta x}\right),$$

$$0 < \alpha_{i}, \beta_{i} < N_{i} - 1 \text{ for } i=1,2,3.$$
(D2)

Given the above, the one-sided power spectrum is defined as [PFTV]

$$P_{\alpha_1,\alpha_2\alpha_3} = \frac{1}{(N_1 N_2 N_3)^2} \left[|\widetilde{F}_{\alpha_1,\alpha_2,\alpha_3}|^2 + |\widetilde{F}_{N_1-\alpha_1,N_2-\alpha_2,N_3-\alpha_3}|^2 \right], \quad (D3)$$

for $1 \le \alpha_i \le (\frac{N_i}{2} - 1)$ i=1,2,3. In the special case when one or more of the α_i is either zero or $\frac{N_i}{2}$, then adjustments must be made; in particular,

$$P_{0,0,0} = \frac{2}{(N_1 N_2 N_3)^2} |\widetilde{F}_{0,0,0}|^2,$$

$$P_{\frac{N_1}{2}, \frac{N_2}{2}, \frac{N_3}{2}} = \frac{2}{(N_1 N_2 N_3)^2} |\widetilde{F}_{\frac{N_1}{2}, \frac{N_2}{2}, \frac{N_3}{2}}|^2,$$
(D4)

and similar expressions are used for P_{0,α_2,α_3} , $P_{0,0,\alpha_3}$ etc. Once we have the three-dimensional one-sided power spectrum, we calculate the modes to which the power spectrum corresponds. This is done by comparing the wavelength of the string with the wave number of each point in the power spectrum and putting the contribution into an appropriate bin.

There is a problem associated with this approach to power spectrum analysis. The discrete Fourier transform assumes that the initial data is periodic, which is not necessarily the case for the radiation field in our simulations. The resulting discontinuities at the boundaries can cause spurious harmonics to appear in the spectrum. We overcome this by multiplying the data by a window function, W(x). Window functions should be periodic and fall-off quickly toward zero at the edges. To apply the window function we calculate the discrete Fourier transform of G(x) = W(x)F(x). Using the convolution theorem and the properties of W(x), we can recover the Fourier transform of F(x) as

$$\widetilde{G}_{\beta_1,\beta_2,\beta_3} = \frac{\widetilde{F}_{\beta_1,\beta_2,\beta_3}}{W_{ss}}, \tag{D5}$$

where

$$W_{ss} = \sum_{\alpha_1=1}^{N_1-1} \sum_{\alpha_2=1}^{N_2-1} \sum_{\alpha_3=1}^{N_3-1} \left(\frac{W_{\alpha_1,\alpha_2,\alpha_3}}{N_1 N_2 N_3} \right)^2.$$
 (D6)

The window function $W_{\alpha_1,\alpha_2,\alpha_3}$ is decoupled in each direction, that is, $W_{\alpha_1,\alpha_2,\alpha_3} = W_{\alpha_1}W_{\alpha_2}W_{\alpha_3}$, where each of the W_{α_i} is a one-dimensional window function similar to those described in ref. [H]. After extensive trials, it appeared that the problem was best suited to a Gaussian window function, that is,

$$W_{\alpha_i} = e^{-\beta \left(\alpha_i - \frac{N_i}{2}\right)^2},\tag{D7}$$

where i = 1, 2, 3 and β is comparable to the inverse of the simulation box-length.

References

Lyth1 Lyth, D.H. [1993], 'Dilution of cosmological densities by saxino decay,' Lancaster preprint.

SN Frieman, J., Dimopoulous, S. & Turner, M.S. [1987], 'Axions and Stars,' *Phys. Rev.* **D36**, 2201.

RG Dearbon, D.S.P., Schramm, D.N., Steigman, G. [1986], 'Astrophysical constraints on the coupling of axions, majorons and familons,' *Phys. Rev. Lett.* **56**, 26.

CKLL Copeland, E.J., Kolb, E.W., Liddle, A.R., & Lidesey, J.E. [1993], 'Observing the inflaton potential,' *Phys. Rev. Lett.* **71**, 219.

BSa Battye, R.A., & Shellard, E.P.S. [1993], 'Numerical field theory simulation methods for global topological defects,' in preparation.

BSb Battye, R.A., & Shellard, E.P.S. [1993], 'String radiation backreaction,' in preparation.

LR Lund, F., & Regge, T. [1976], 'Unified approach to strings & vortices with soliton solutions,' *Phys. Rev.* **D14**, 1525.

Tur Turok, N. [1984], 'Grand unified strings and galaxy formation,' *Nucl. Phys.* **B242**, 520.

Bur Burden, C.J. [1985], 'Gravitational radiation from a particular class of cosmic strings,' *Phys. Lett.* **164B**, 277.

EM Engquist, B., & Majda, A. [1977], 'Absorbing boundary conditions for the numerical simulation of waves,' *Mathematics of Computation* **31**, 629.

EH Engquist, B., & Halpren, L. [1990], 'Long time behaviour of absorbing boundary conditions,' *Mathematical Methods in the Applied Sciences* **13**, 189.

BJR Bamberger, A., Joly, P., & Roberts, J.E. [1990], 'Second order boundary conditions for the wave equation: A solution for the corner problem,' SIAM Journal of Numerical Analysis 27, 323.

W Welch, P.D. [1967], 'The use of fast fourier transform for the estimation of power spectra: A method based on time averaging over shorth, modified periodograms,' *IEEE Transactions on Audio and Electroacoustics* **AU-15**, 70.

H Harris, F.L. [1978], 'On the use of window for harmonic analysis with the discrete fourier transform,' *Proceedings of the IEEE* **66**, 51.

- M McClellan J.H. [1982], 'Multidimensional spectral estimation,' *Proceedings of the IEEE* **70**, 1029.
- PFTV Press, W.H., Flannery, B.P., Teukolsky, S.A., & Vetterling, W.T. [1986], Numerical recipes (Cambridge University Press).
 - Car Carter, B. [1993], 'Kalb-Ramond coupled string vortex dynamics in a relativistic superfluid,' DARC preprint.
 - AT Albrecht, A., & Turok, N. [1989], 'Evolution of cosmic string networks,' *Phys. Rev.* **D40**, 973.
 - BB Bennett, D.P., & Bouchet, F.R. [1990], 'High resolution simulations of cosmic string evolution: network evolution,' *Phys. Rev.* **D41**, 2408.
 - AShe Allen, B., & Shellard, E.P.S. [1990], 'Cosmic string evolution—a numerical simulation,' *Phys. Rev. Lett.* **64**, 119.
- AShe2 Allen, B., & Shellard, E.P.S. [1992], 'Gravitational radiation from a cosmic string network,' *Phys. Rev.* **D45**, 1898.
 - AS Abbott, L.F., & Sikivie, P. [1983], 'A cosmological bound on the invisible axion,' *Phys. Lett.* **120B**, 133.
 - PQ Peccei, R.D., & Quinn, H.R. [1977], 'CP conservation and the presence of pseudoparticles,' *Phys. Rev. Lett.* **38**, 1440; *Phys. Rev.* **D16**, 1791.
- HagS Hagmann, C., & Sikivie, P. [1991], 'Computer simulations of the motion and decay of global strings,' *Nucl. Phys.* **B363**, 247.
- HarS Harari, D., & Sikivie, P. [1987], 'On the evolution of global strings in the early universe,' *Phys. Lett.* **195B**, 361.
- Sika Sikivie, P. [1982], 'Axions, domain walls and the early universe,' *Phys. Rev. Lett.* **48**, 1156.
- Sikb Sikivie, P. [1992], 'Dark matter axions', Proceedings of First I.F.T. Workshop on *Dark Matter*, University of Florida, Gainseville, Feb. 14–16, 1992.
- Dava Davis, R.L. [1985], 'Goldstone bosons in string models of galaxy formation,' *Phys. Rev.* **D32**, 3172.
- Davb Davis, R.L. [1986], 'Cosmic axions from cosmic strings,' *Phys. Lett.* **180B**, 225.
- DSa Davis, R.L., & Shellard, E.P.S. [1989], 'Do axions need inflation?,' Nucl. Phys. **B324**, 167.
- DSb Davis, R.L., & Shellard, E.P.S. [1988], 'Antisymmetric tensors and spontaneous symmetry breaking,' *Phys. Lett.* **214B**, 219.
- DSc Davis, R.L., & Shellard, E.P.S. [1989], 'Global strings and superfluid vortices,' *Phys. Rev. Lett.* **63**, 2021.
- Sa Shellard, E.P.S. [1986], 'Axionic domain walls & cosmology', in Proceedings of the 26th Liege International Astrophysical Colloquium, *The Origin and Early History of the Universe*, Demaret, J., ed. (University de Liege).
- Sb Shellard, E.P.S. [1990], 'Axion strings and domain walls', in *Formation and Evolution of Cosmic Strings*, Gibbons, G.W., Hawking, S.W., & Vachaspati, V., eds. (Cambridge University Press).
- Sc Shellard, E.P.S. [1987], 'Cosmic string interactions,' Nucl. Phys. B283, 624.
- Sd Shellard, E.P.S. [1992], 'The numerical study of topological defects', in *Approaches to Numerical Relativity*, d'Inverno, R., ed. (Cambridge University Press).

- PWW Preskill, J., Wise, M.B., & Wilczek, F. [1983], 'Cosmology of the invisible axion,' Phys. Lett. 120B, 127.
 - Wil Wilczek, F. [1978], 'Problem of strong P and T invariance in the presence of instantons,' *Phys. Rev. Lett.* **40**, 279.
 - Wei Weinberg, S. [1978], 'A new light boson?,' Phys. Rev. Lett. 40, 223.
 - KR Kalb, M. & Ramond, P. [1974], 'Classical direct interstring action,' *Phys. Rev.* **D9**, 2273.
 - KT Kolb, E.W., & Turner, M.S. [1990], *The Early Universe* (Addison-Wesley, Redwood City, California).
 - VE Vilenkin, A., & Everett, A.E. [1982], 'Cosmic strings and domain walls in models with Goldstone and pseudo-Goldstone bosons,' *Phys. Rev. Lett.* 48, 1867.
 - VVa Vilenkin, A., & Vachaspati, T. [1987], 'Radiation of Goldstone bosons from cosmic strings,' *Phys. Rev.* **D35**, 1138.
 - VVb Vachaspati, T., & Vilenkin, A. [1985], 'Gravitational radiation from cosmic strings,' *Phys. Rev.* **D31**, 3052.
 - Wit Witten, E. [1985], 'Cosmic superstrings,' Phys. Lett. 153B, 243.
 - Hina Hindmarsh, M.B. [1990], 'Gravitational radiation from kinky infinite strings,' *Phys. Lett.* **251B**, 28.
 - Hinb Hindmarsh, M.B. [1993], private communication
 - Saka Sakellariadou, M. [1990], 'Gravitational waves emitted from infinite strings,' *Phys. Rev.* **D42**, 354.
 - Sakb Sakellariadou, M. [1991], 'Radiation of Nambu-Goldstone bosons from infinitely long cosmic strings,' *Phys. Rev.* **D44**, 3767.
 - VS Vilenkin, A. & Shellard, E.P.S. [1993], Cosmic strings and other topological defects (Cambridge University Press(in press)).
 - PRS Press, W.H., Ryden, B.S., & Spergel, D.N. [1989], 'Dynamical evolution of domain walls in an expanding universe,' Ap. J. 347, 590.
 - DQ Dabholkar, A., & Quashnock, J.M. [1990], 'Pinning down the axion,' Nucl. Phys. **B333**, 815.
- GKPB Gradwohl, B., Kalbermann, G., Piran, T., & Bertschinger, E. [1990], 'Global strings and superfluid vortices: analogies and differences,' *Nucl. Phys.* **B338**, 371.
 - Lyta Lyth, D.H. [1992], 'Estimates of the cosmological axion density,' *Phys. Lett.* **275B**, 279.